INTERFACE FOCUS

rsfs.royalsocietypublishing.org

Review

Cite this article: Holmes WR, Golding AE, Bement WM, Edelstein-Keshet L. 2016 A mathematical model of GTPase pattern formation during single-cell wound repair. *Interface Focus* **6**: 20160032. http://dx.doi.org/10.1098/rsfs.2016.0032

One contribution of 13 to a theme issue 'Coupling geometric partial differential equations with physics for cell morphology, motility and pattern formation'.

Subject Areas:
biomathematics

Keywords:
Cdc42, Rho, protein kinase C, reaction–diffusion model, guanosine nucleotide dissociation inhibitors, wound repair

Author for correspondence:
William R. Holmes
e-mail: william.holmes@vanderbilt.edu

A mathematical model of GTPase pattern formation during single-cell wound repair

William R. Holmes[1], Adriana E. Golding[2], William M. Bement[2] and Leah Edelstein-Keshet[3]

[1]Department of Physics and Astronomy, Vanderbilt University, Nashville, TN, USA
[2]Cellular and Molecular Biology Program, Laboratory of Cell and Molecular Biology, Department of Zoology, University of Wisconsin, Madison, WI, USA
[3]Department of Mathematics, University of British Columbia, Vancouver, BC, Canada

Rho GTPases are regulatory proteins whose patterns on the surface of a cell affect cell polarization, cell motility and repair of single-cell wounds. The stereotypical patterns formed by two such proteins, Rho and Cdc42, around laser-injured frog oocytes permit experimental analysis of GTPase activation, inactivation, segregation and crosstalk. Here, we review the development and analysis of a spatial model of GTPase dynamics that describe the formation of concentric zones of Rho and Cdc42 activity around wounds, and describe how this model has provided insights into the roles of the GTPase effector molecules protein kinase C (PKCβ and PKCη) and guanosine nucleotide dissociation inhibitor (GDI) in the wound response. We further demonstrate how the use of a 'sharp switch' model approximation in combination with bifurcation analysis can aid mapping the model behaviour in parameter space (approximate results confirmed with numerical simulation methods). Using these methods in combination with experimental manipulation of PKC activity (PKC overexpression (OE) and dominant negative conditions), we have shown that: (i) PKCβ most probably acts by enhancing existing positive feedbacks (from Rho to itself via the guanosine nucleotide exchange factor domain of Abr, and from Cdc42 to itself), (ii) PKCη most probably increases basal rates of inactivation (or possibly decreases basal rates of activation) of Rho and Cdc42, and (iii) the graded distribution of PKCη and its effect on initial Rho activity accounts for inversion of zones in a fraction (20%) of PKCη OE cells. Finally, we speculate that GDIs (which sequester GTPases) may have a critical role in defining the spatial domain, where the wound response may occur. This paper provides a more thorough exposition of the methods of analysis used in the investigation, whereas previous work on this topic was addressed to biologists and abbreviated such discussion.

1. Introduction

Biological pattern formation has been studied mathematically since the seminal work of Alan Turing in 1952 [1]. Originally concerned with macroscopic patterns in morphogenesis, his work and that of others showed that chemical prepatterns can engender regular placement of body parts, leaves on plants, bristles or other periodic biological structures [2]. As early as 1972, it was proposed by Gierer & Meinhardt [3] that related mechanisms of short-range activation and long-range inhibition could also explain intracellular patterns and account for polarity of cells, a notion that was expanded more than 25 years later in a groundbreaking paper by Meinhardt [4]. Over the past two decades, research on chemical patterns and chemical polarization in cells has blossomed, providing fertile grounds for both experimental and theoretical contributions.

Broadly speaking, this field has addressed two challenges: the first has been to identify the molecular players that participate in the pattern-forming system in cell polarity and to experimentally demonstrate the existence of hypothesized 'local excitation, global inhibition' [5–7] or generalized Turing interactions [8]. A second line of inquiry has been to use phenomenological observations of

THE ROYAL SOCIETY PUBLISHING

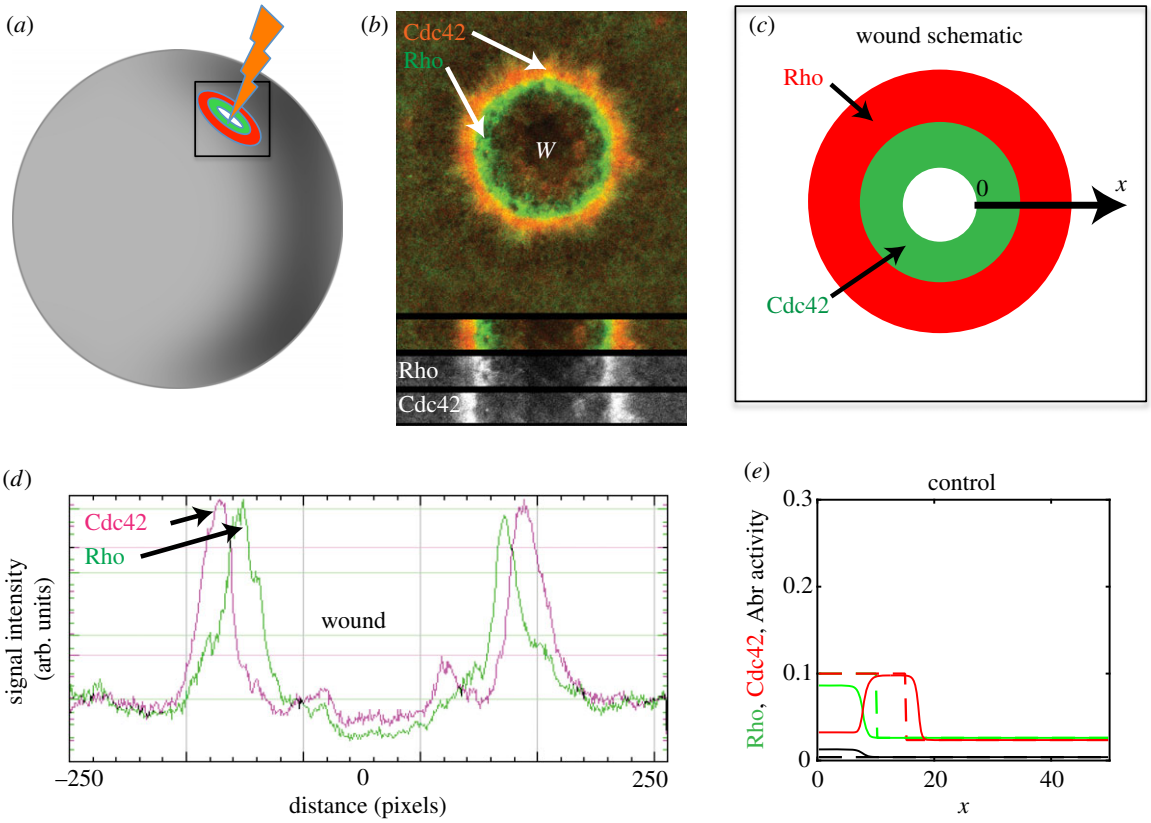

Figure 1. GTPase pattern in single-cell wound. (*a*) A frog egg (Xenopus oocyte ≈1000 µm in diameter) is punctured by a laser as described in [18], leading to development of concentric zones of GTPase activity on its surface: Rho (green) and Cdc42 (red). Consistent red/green colour scheme is used throughout figures. (*b*) Experimental data showing Rho and Cdc42 surrounding a single-cell wound (top) and in one-dimensional slices across the wound diameter. (*c*) Our one-dimensional spatial geometry for the model wound; x is distance from wound edge. (*d*) Line scan of Cdc42 and Rho fluorescence intensity observed experimentally across the diameter of the wound. (*e*) Simulation of the model showing the predicted spatial distribution of Rho, Cdc42 and Abr (black) activities as a function of distance from wound, x, at $t = 30$ s. (Online version in colour.)

cellular patterns, mutants and drug-induced changes to decipher underlying mechanisms at play in observed pattern formation of various sorts in the cell. This review paper fits into the latter category. We use the observed patterns formed by Rho GTPases (Rho and Cdc42) on the surface of a cell after injury, to show how features of the underlying molecular network that creates that pattern could be deduced. As we will show, a combination of experiment and theory helped to refine our understanding of how activation and inhibition combine to regulate and drive a pattern of functional significance in healing a cellular injury. While many of these conclusions were published previously in a format suitable for biological readers [9], our purpose here is to showcase the mathematical methods that led to our inferences. We hope that these techniques may be of benefit to other modellers.

Rho GTPases are a family of proteins that regulate the dynamics of the actin cytoskeleton. Their roles in cell polarization, shape change and motility have long been recognized [10,11]. Upon activation by guanine nucleotide exchange factors (GEFs), these proteins are recruited to the plasma membrane where they bind to and activate their target (effector) proteins. They can be inactivated by GTPase-activating proteins (GAPs), whereupon they can bind to guanosine nucleotide dissociation inhibitors (GDIs), which sequester them in an inactive state that diffuses rapidly in the cytosol [12–14]. Three common Rho GTPases are: Cdc42, Rac and Rho. Cdc42 activates N-WASP, which promotes actin filament branching, nucleation and assembly (via Arp2/3), whereas Rho activates Rho kinase, which leads to actomyosin assembly and myosin contraction. By virtue of their positive and negative interactions with one another [15], Rho GTPases form a network with spatial pattern-forming properties [16]. Both the dynamics of and the spatial distributions of Rho proteins are key to their ability to regulate facets of cell behaviour [17]. The interplay of Rho proteins, their GEFs, GAPs, GDIs and other effectors are subject of intense biological study, though it is often challenging to untangle the network of crosstalk and downstream effects. An important challenge is to use the observed spatial pattern of GTPase activity to elucidate the underlying interactions responsible for that organization. Here, we report on one example of such experiment–theory research.

Single-cell wounds have proved to be a useful model system in which to study Rho GTPase signalling. Upon wounding, the surface of the frog egg (Xenopus oocyte) undergoes a stereotypical response involving Rho GTPases (figure 1): Rho and Cdc42 are quickly activated near the wound, and segregate within tens of seconds into concentric rings of activity (hereon termed ‘zones’). The fluorescence intensity is high within the zones and low (background) elsewhere. The Cdc42 zone surrounds the Rho zone, which in turn surrounds the wound edge [18,19]. This spatial pattern results in the recruitment of actin filaments and myosin-2, which assemble into a contractile ring that closes over the site of damage [19,20]. An important participant in this process is the dual GEF–GAP Abr which activates Rho and inactivates Cdc42 and thereby promotes zone segregation [21,22]. Because the location and timing of wounds are controlled by the investigator, wound elicited GTPase activation provides a powerful alternative to more complex models of network interaction analysis such as those provided by cell motility or cell division.

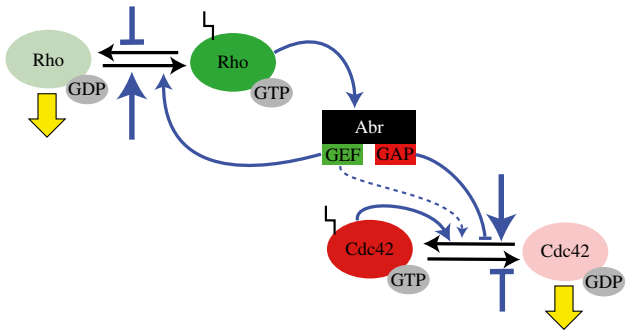

Figure 2. Schematic diagram of the GTPase signalling network. The GTPases Rho and Cdc42 in their active (GTP-bound) and inactive (GDP-bound) forms. Horizontal black arrows represent GTPase (in)activation by unspecified GAPs and GEFs. Rho enhances the activity of the GEF–GAP Abr, which then inactivates Cdc42, and activates both Rho and (to a weak extent) Cdc42. Thick vertical blue arrows depict plausible effects of PKCβ on basal or feedback rates of (in)activation. PKCη influence (not shown) is opposite that of PKCβ. Yellow arrows denote sequestration of inactive GTPases by GDI. The mathematical model allows us to distinguish between competing hypotheses for the actions of the PKCs and for the role of GDI in defining a playing field for pattern formation to occur. (Online version in colour.)

Mathematical modelling has helped to focus a number of questions that experiment and theory can address in this system. Such questions include the following:

(1) What initiates patterning?
(2) What causes the Rho and Cdc42 zones to segregate?
(3) What prevents GTPase zones from spreading outward? That is, what defines the 'playing field' within which GTPase activity patterns can form?
(4) How can we understand the roles of other players that damp or accentuate one or another zone or background intensity?

In previous work, we addressed (2–4) in the context of a PDE model for Rho, Abr and Cdc42 [23]. A schematic of the basic system is shown in figure 2. More recently, there has been evidence for lipid-dependent regulation of the wounds [24]. Of particular interest has been the involvement of the antagonistic protein kinases eta and beta (PKC β and η) [9,25]. The former activates Rho and Cdc42, whereas the latter inhibits them, but the exact mechanism is unclear. This led to several additional questions, such as: How do PKCs eta and beta affect the system? One puzzling observation is that PKCη overexpression (OE) dampens the Rho zone in ≈80% of cells, but in the remaining ≈20%, it causes the Cdc42 and Rho zones to trade places (zone inversion). We asked how this could be explained.

2. Description of models

In order to explore the spatio-temporal interactions based on the schematic in figure 2, we formulated a set of PDEs for the key signalling components that direct the wound response, Rho, Cdc42 and Abr. We take $x = 0$ at the wound edge, as shown in figure 1 and model the period of time 48–78 s post-wounding, when the patterns emerge ($t = 0$ corresponds to 48 s post-wounding). Earlier events such as calcium-dependent initiation are not in the scope of this model.

For a typical GTPase, let $G(x, t)$ be the concentration of active GTPase on the cell membrane at position x and time t, and let G_i be the concentration of inactive GTPase in the cytosol (available to be activated). Rho GTPases are activated by GEFs, and inactivated and sequestered by GAPs and GDIs, respectively. The general dynamics of the active GTPases are encoded in model equations of the form

$$\frac{\partial G}{\partial t} = (\text{Activation rate}) \cdot G_i - (\text{Inactivation rate}) \cdot G + D\Delta G,$$

where

$$\text{Activation rate} = b_G + F(G_1, G_2, \ldots),$$
$$\text{Inactivation rate} = d_G + H(G_1, G_2, \ldots).$$

Here $D\Delta C$ is diffusion of active GTPase in the plasma membrane. Terms such as b_G, d_G depict basal rates while the remaining terms account for feedbacks and crosstalk between various GTPases and their regulators. For example, Abr acts as a GEF for Rho and GAP/GEF for Cdc42 (figure 2), and so appears in the model equations. In addition to basal activation and inactivation rates, some form of feedback stemming from GTPase crosstalk in either one or both of the above is required to account for coexistence of low background activity levels throughout the egg surface as well as high activity levels within the 'zones' next to the wound. (Restated mathematically, the model has to be sufficiently nonlinear to display bistable behaviour.) Typically, such feedbacks are represented by sigmoidal Hill functions (for F, H), a commonplace assumption in models of signalling circuits in the cell. Such terms depict the fact that the activation or inactivation of one GTPase by another is nonlinear and saturating. While feedbacks are likely present in both activation and inactivation kinetics, in practice, it is not possible to disentangle the two when the underlying molecular mechanisms are unknown. We thus arbitrarily choose H to be constant, and assume nonlinearity in the activation term F. Similar behaviour is obtained if F is constant and H is a decreasing Hill function [25].

We define $R(x, t)$ and $C(x, t)$ as the levels of Rho and Cdc42 activity at a distance x from the wound edge at time t, and $A(x, t)$ as the level of Abr activity. The equations that track these variables are then:

$$\frac{\partial R}{\partial t} = \left(b_R + \gamma_{AR}\frac{A^6}{K_R^6 + A^6}\right)R_i - \bar{d}_R R + D\Delta R, \tag{2.1a}$$

$$\frac{\partial C}{\partial t} = \left(b_C + \gamma_{AC} \cdot A + \gamma_C \frac{C^6}{K_C^6 + C^6}\right)C_i - (\bar{d}_C + d_{AC} \cdot A)C + D\Delta C \tag{2.1b}$$

and

$$\frac{\partial A}{\partial t} = \gamma_{RA} \cdot R - d_A \cdot A + D\Delta A, \tag{2.1c}$$

where $D\Delta C$, $D\Delta R$ and $D\Delta A$ represent diffusion of active GTPases and of Abr in the plasma membrane. We use no-flux boundary conditions at $x = 0, \infty$ and step-function initial conditions (shown as dashed lines in figures 3*e,f* and 4*d*).

In equations (2.1*a*,*b*), b_R and b_C are the basal rates of Rho and Cdc42 activation, respectively. The Hill function $(\gamma_{AR}A^6/[K_R^6 + A^6])$ is the rate of activation of Rho by the Abr-GEF motif (with typically $n = 6$). As Abr acts both as GAP and GEF for Cdc42, we include terms $(\gamma_{AC} \cdot A)$ for the Abr-GEF activation, and $(d_{AC} \cdot A)$ for the Abr-GAP inactivation rates of Cdc42. We also model positive feedback of Cdc42 on its own activation rate $(\gamma_C C_a^6/[K_C^6 + C_a^6])$. Beyond that, we cannot experimentally decompose all distinct components of the inactivation pathways. Hence we have used

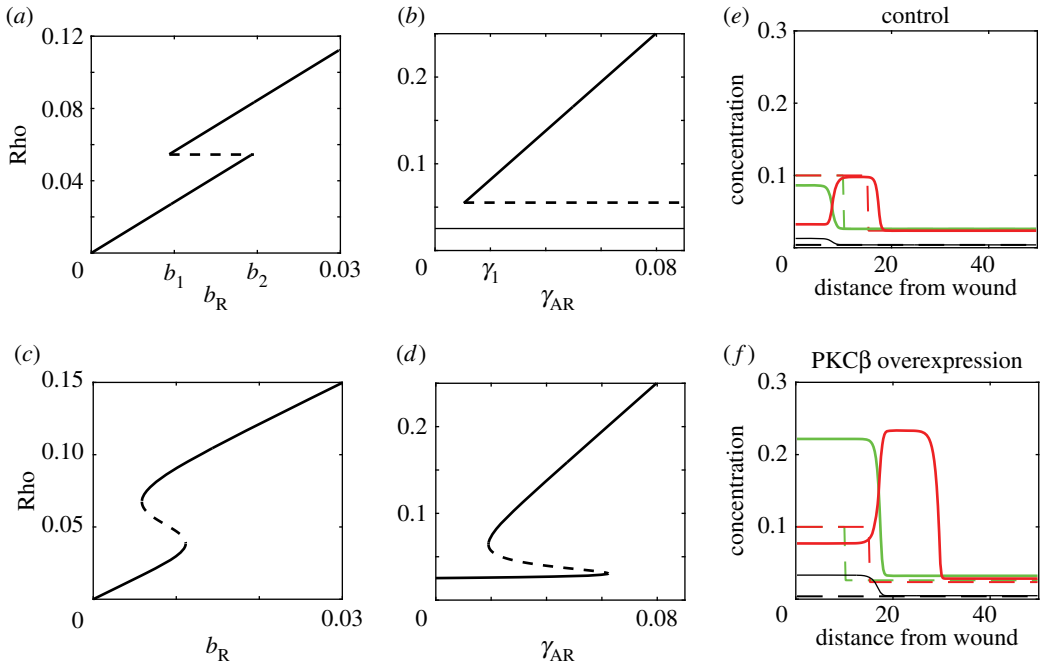

Figure 3. Effect of PKCβ. (*a–d*) Bifurcation diagrams for the well-mixed Rho–Abr subsystem showing Rho intensity versus basal (b_R) and feedback-induced (γ_{AR}) activation rates. The sharp switch approximation in (*a,b*) leads to analytic expressions for bifurcation points b_i, γ_i in equation (3.2); numerical bifurcation analysis of the continuous (unapproximated) system (*c,d*) verifies the results. (*e,f*) One-dimensional spatial simulations of the reaction diffusion system in the control (*e*) and in PKCβ OE (*f*) conditions. Dashed lines represent initial conditions, and solid lines show the spatial profiles 20 s later. In all panels, parameters are as in table 1 with $\bar{d}_R = 1.1$ and $\bar{d}_C = 0.4741$. To mimic PKCβ OE in (*f*), γ_{AR} and γ_C are multiplied by a factor of 2. (Online version in colour.)

the notation $\bar{d}_R$, $\bar{d}_C$ to represent their aggregate actions. Such parameters could in principle be decomposed into specific terms such as

$$\left.\begin{aligned} \bar{d}_R &= d_R + d_{\eta R}\cdot\eta + d_{GR}\cdot G \\ \text{and}\quad \bar{d}_C &= d_C + d_{\eta C}\cdot\eta + d_{GC}\cdot G, \end{aligned}\right\} \qquad (2.1d)$$

where we have explicitly separated terms for basal rates of inactivation (d_R and d_C), inactivation due to PKCη-mediated pathways ($d_{\eta R}$, $d_{\eta C}$), and sequestration of GTPases by the Rho-GDI ($d_{\eta R}$, $d_{\eta C}$). (See discussion of these effects later on.)

The values, meanings and units of all parameters are given in table 1. It is worth commenting on several simplifications used in constructing the model. (i) The wound is small (≈10 µm) relative to the whole cell (≈1000 µm) so that the pattern that forms does not deplete the cellular GTPase reserves. Furthermore, diffusion in the bulk, where inactive forms reside, can rapidly replenish their local levels. Hence we can consider the concentrations of inactive GTPases (R_i, C_i) as roughly constant. Note that this is in distinction with cell polarization patterns, where we have argued that depletion of the inactive GTPases plays a role in stabilizing a polar pattern [26,27]. (ii) Since GDIs are also cytosolic, at first, we will consider their concentration as spatially uniform by the same argument. This is refined in §3.5. (iii) The full problem in two dimensions has radial symmetry and also entails a transport term due to flow of material towards the wound edge. However, for the purpose of addressing the pattern-forming system and understanding crosstalk, we can study the model with a static edge and one-dimensional spatial GTPase profiles. See [23] for a fuller treatment of the two-dimensional model and the contracting wound edge.

3. Results

Wound healing is a transient phenomenon, where zones of regulatory activity form, move inward with closure of the wound, and are finally extinguished. While this is a dynamic process, steady-state analysis provides important information about the process. In particular, the formation of 'zones' of high activities near the wound implies model bistability, since these zones coexist with a low activity background.

From figure 2, it is apparent that the model can be decomposed into two subsystems: a Rho–Abr and a Cdc42 subsystem. Abr-GEF/GAP activity mediates positive feedback from Rho to its own activation, and negative feedback from Rho to Cdc42. Together, these actions of Abr account for formation and enhancement of the Rho zone and its exclusion of Cdc42 activity. However, the Rho–Abr subsystem receives no direct inputs from Cdc42 in the model. Analysing each subsystem on its own allows us to determine how each operates individually. We used a combination of qualitative methods and simulations to accomplish this.

3.1. Basic model

A basic Rho–Abr–Cdc42 model with two-dimensional spatial geometry (and radial coordinates with respect to wound centre), developed by Simon *et al.* [23], led to several conclusions. First, a positive feedback loop from Cdc42 to its own activation is essential for Cdc42 zone formation ($\gamma_C \neq 0$). Second, the basic interactions shown in figure 2, together with Hill activation kinetics leads to spontaneous separation of the Rho and Cdc42 zones. Third, the model is predictive and explanatory of several manipulations and mutants, including OE of Abr, GEF-dead and GAP-dead Abr, and Rho inactivation (by C3 exo-transferase injection). The existence, stability and magnitudes of multiple steady states in model variants explain how such manipulations lead to the experimentally observed changes. Finally, two wounds at various distances apart lead

Table 1. Synopsis of the basic 'control' (WT) parameter values used in simulations for our model. All parameters are based on the original model by Simon *et al*. [23], with the exception of parameters influenced by PKCη, $d_{\eta,C}$ and $d_{\eta,R}$. Owing to lack of relevant data, parameters associated with the influence of GDI on Rho (d_{GR}) and Cdc42 (d_{GC}) (introduced for illustrative purposes only in equations (2.1*d*)) are folded into d_R and d_C, respectively. See text for more details.

parameter	meaning	value	units
b_R	basal Rho activation rate	0.009	s^{-1}
γ_{AR}	Abr-induced Rho feedback strength	0.023	s^{-1}
K_R	Abr level for (1/2)-max feedback to Rho	0.0082	μmol
R	amount of inactive Rho	3.1	μmol
d_R	Rho basal inactivation rate	1.1	s^{-1}
$d_{\eta R}$	PKCη-induced Rho inactivation rate	1	s^{-1} μmol^{-1}
b_C	basal Cdc42 activation rate	0.0015	s^{-1}
γ_{AC}	strength of Abr mediated Cdc42 activation	2	s^{-1} μmol^{-1}
γ_C	Cdc42 positive feedback strength	0.031	s^{-1}
K_C	Cdc42 level for (1/2)-max feedback	0.055	μmol
C	amount of inactive Cdc42	2.4	μmol
d_C	Cdc42 basal inactivation rate	0.47	s^{-1}
$d_{\eta C}$	PKCη-induced Cdc42 inactivation rate	1	s^{-1} μmol^{-1}
d_{AC}	Abr-GAP mediated Cdc42 inactivation rate	127.4	s^{-1} μmol^{-1}
γ_{RA}	feedback from Rho to Abr activation rate	0.1	s^{-1}
d_A	Abr inactivation/decay rate	0.67	s^{-1}
D	protein diffusion coefficient along membrane	0.1	$\mu m\ s^{-2}$

to overlapping patterns in two-dimensional model simulations that agree with experimental observations. In short, experiments and model concur in most broad qualitative features of the pattern formation.

3.2. Deciphering the effects of GTPase modulators PKCβ and PKCη

In more recent experiments, it has emerged that protein kinase C beta and eta (PKCβ, PKCη) affect GTPase patterns after cell-wounding. The PKCs are recruited to wounds quickly by calcium and the lipid diacylglycerol (DAG) (PKCβ) or DAG alone (PKCη). Spatial localizations of PKCs are however different [24]. PKCβ overlaps the Rho and Cdc42 zones where it enhances both GTPase activities, whereas PKCη is restricted to a narrow region near the wound edge where it inhibits both. We asked whether PKCs act by damping or accelerating the existing basal rates or by amplifying existing feedbacks. We used mathematical modelling to address this issue in [9].

Upon introducing new players to the model, we could either choose to expand the model to include new (dynamic) variables, or we could treat these players as effective parameter variations. The former comes at the expense of adding complexity to the model, while the latter could miss some important dynamics. We chose the latter more parsimonious approach which proves easier to analyse while providing useful insights. This raises the question of which components of the system (and therefore which parameters) are targeted by the PKCs. To address this, we used data for OE and dominant negative (DN) manipulations of both PKCs in combination with modelling to identify the likely PKC targets.

To do so, we consider regimes where the Rho–Abr subsystem is bistable, to account for coexistence of zones and background states. We then examined bifurcations with respect to b_R, b_C, $\bar{d}_R$, $\bar{d}_C$, γ_{AR} and γ_C, all of which are potential PKCβ/PKCη targets, paying particular attention to the qualitative and semi-quantitative changes in both background (low steady state) and zone intensities (high steady state) as these parameters are varied. Importantly, we used the following observations:

(O1) For PKCβ OE, both Rho and Cdc42 zones are significantly brighter while background activity is the same as in the control; similarly, for PKCβ DN, both Rho and Cdc42 zones are suppressed, with unchanged background activity.
(O2) For PKCη DN, both Rho and Cdc42 zone intensities are the same as control, whereas both their background activities are higher.
(O3) For PKCη OE, 80% of cells show a loss of the Rho zone, but the Cdc42 zone intensity and localization remain similar to control.
(O4) For PKCη OE, 20% of the cells retain both zones, but the Rho zone is outside of the Cdc42 zone. This latter puzzling behaviour is termed 'zone inversion'.

Details of the analysis is concentrated in §3.3. We examined the following hypotheses:

(H1) PKCβ enhances basal GEF activity (b_R, b_C).
(H2) PKCβ enhances feedback strength (γ_{AR} and γ_C).
(H3) PKCη either increases GTPase inactivation ($\bar{d}_R$, $\bar{d}_C$) or suppresses GTPase basal activation (b_R, b_C).
(H4) PKCη influences feedback strengths (γ_{AR}, γ_C).

Several conclusions are summarized below. Upon analysing the dependence of both zone brightness and background GTPase activation levels with respect to parameters, we

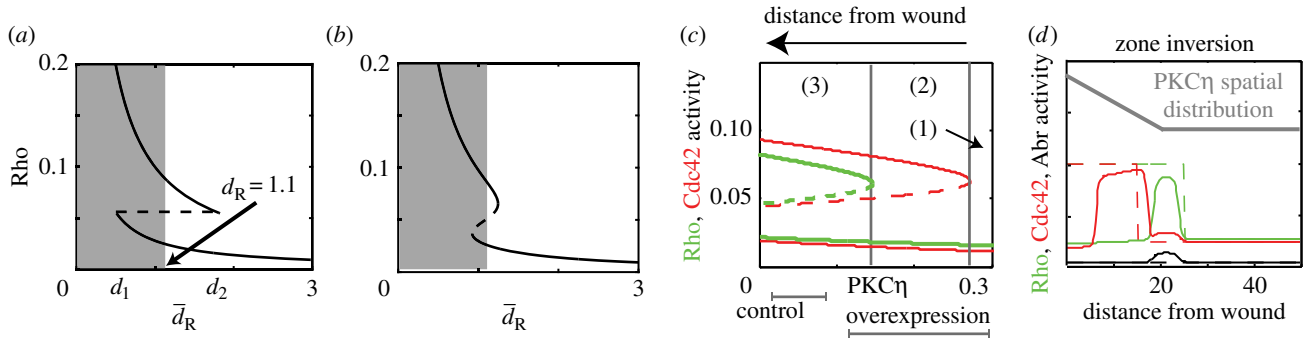

Figure 4. Effect of basal rates of inactivation and of PKCη. (*a*) Bifurcation analysis of the sharp switch, well-mixed Rho/Abr subsystem with respect to the aggregate Rho inactivation rate ($\bar{d}_R$). (A fixed basal inactivation level d_R would imply that a region near the origin, shaded grey, would be experimentally inaccessible in PKCη manipulations.) (*b*) As in (*a*), but for the continuous (unapproximated) model. (*c*) Bifurcation analysis of Rho and Cdc42 intensities with respect to $\eta =$ PKCη level jointly influencing Rho and Cdc42 inactivation rate, as per equation (2.1*d*). Here, η is the bifurcation parameter and $G = 0$ in equation (2.1*d*). Three regimes are: (1) no zone possible, (2) Cdc42 but not Rho zone possible, (3) both Rho and Cdc42 zones possible. (*d*) Inversion of the Rho and Cdc42 zones can occur under the following model conditions: PKCη is over-expressed and spatially distributed (grey curve) and the Rho initial condition is broad. The values of η (max−min) spanned by the piecewise PKCη spatial distribution for typical control and typical PKCη OE wound are illustrated underneath (*c*). The control wound leads to a region permissive to both Rho and Cdc42, whereas the region adjoining a PKCη OE wound is permissive to Cdc42. (Online version in colour.)

conclude based on observations (O1)–(O3) that (H1) and (H4) are unlikely. Overall, our analysis strongly suggests that PKCβ enhances feedback strengths (H2) while PKCη accelerates GTPase inactivation (H3). We explain these conclusions next.

3.3. Details of model analysis for the effect of PKCβ

In this section, we provide details and analysis supporting the conclusions outlined in §3.2. We use experimental data about existence or absence of zones (qualitative observations) as well as the relative intensities of zones and backgrounds (semi-quantitative observations) under PKCβ/PKCη OE and DN manipulations to infer the likely targets (model parameters) of the PKCs.

Analysis is based on several simplifications. (i) We treat Rho–Abr and Cdc42 as two subsystems, as previously described. (ii) The well-mixed variant of this PDE system is used to analyse the distinct steady-state regimes of the system. (iii) We approximate the Hill function in equation (2.1*a*) by a 'sharp switch' (step function that switches on when $A = K_R$). This is equivalent to the Hill coefficient limit $n \to \infty$ and allows for closed-form analytic steady-state solutions that readily reveal the bifurcation structure. (iv) We use the steady-state Abr level $A = R \cdot (\gamma_{RA}/d_A)$ in equation (2.1*a*) to reduce the R-A subsystem to a single equation in R. (v) We confirm these approximate analytic results with full numerical bifurcation analysis and numerical solutions of the original PDE model. (See figures 3 and 4, and details below.)

In the sharp switch limit of the well-mixed Rho–Abr subsystem, explicit formulae for two possible (stable) steady states are

$$R_{ss} = \begin{cases} R_{low} := \dfrac{b_R}{\bar{d}_R} R_i, & \text{for } R_{low} < R_{crit} \\ R_{high} := \dfrac{b_R + \gamma_{AR}}{\bar{d}_R} R_i, & \text{for } R_{high} > R_{crit}, \end{cases} \tag{3.1}$$

$$\text{where} \quad R_{crit} = \frac{d_A}{\gamma_{RA}} K_R.$$

These values represent, respectively, the low background Rho activity levels, and the high activity level inside the Rho 'zone' adjacent to the wound. (An unstable steady state separates these two states.) Formulae (3.1) produce bifurcation diagrams for Rho activity (R) with respect to parameters. In figure 3*a*,*b*, we plot steady-state R against basal (b_R) and feedback (γ_{AR}) activations. (Comparison with the numerical continuation of the original well-mixed model, figure 3*c*,*d*, verifies that the 'sharp switch' approximation is reasonable.) We can also identify parametric criteria for bistability, namely

$$\left.\begin{aligned} &b_1 < b_R < b_2 \quad \text{where } b_1 = b_2 - \gamma_{AR}, \ b_2 = \frac{d_A \bar{d}_R}{\gamma_{RA}} \frac{K_R}{R_i}, \\ &d_1 < d_R < d_2 \quad \text{where } d_1 = \frac{b_R \gamma_{RA}}{d_A} \frac{R_i}{K_R}, \ d_2 = \frac{(b_R + \gamma_{AR}) \gamma_{RA}}{d_A} \frac{R_i}{K_R}, \\ &\gamma_1 < \gamma_{AR} < \gamma_2 \quad \text{where } \gamma_1 = \frac{d_A \bar{d}_R}{\gamma_{RA}} \frac{K_R}{R_i} - b_R, \ \gamma_2 = \infty. \end{aligned}\right\} \tag{3.2}$$

Figure 3*a*,*b* indicates that zone brightness (upper branches) increases with both b_R and γ_{AR}. By contrast, background levels (lower branches) are sensitive to the basal activation rate b_R, but not to the feedback strength γ_{AR}. (These conclusions are confirmed by the numerical continuation of the full well-mixed model shown in figure 3*e*,*f*.)

Based on Observation (O1), we take this result to mean that the effect of PKCβ OE is consistent with an increase in the feedback parameter γ_{AR}, rather than the basal activation rate b_R. Similar analysis of the Cdc42 subsystem (omitted for brevity) combined with Observation (O1) for Cdc42 leads to similar results. We conclude that PKCβ acts on both Rho and Cdc42 feedback parameters—increasing those feedback strengths γ_{AR}, γ_C for PKCβ OE and damping it for PKCβ DN. We do not rule out other pathways, nor can we identify molecular details for the feedback mechanism in the case of Cdc42.

The full model PDEs were simulated numerically for the parameter set in table 1. Profiles of Rho (green), Cdc42 (red) and Abr (black) are shown in figure 3*e* for the control and figure 3*f* for PKCβ OE. These spatial profiles are in good agreement with observed experimental data.

3.4. Zone inversion reveals a potential role for PKCη

In opposition to PKCβ, PKCη either

(I) promotes inactivation or
(II) suppresses the activation of Rho and/or Cdc42.

We explored the possibilities that it acts by depressing feedback parameters γ_{AR}, γ_C, or by increasing basal inactivation represented by $\bar{d}_R$ and $\bar{d}_C$. From previous analysis (figure 3*b*,*d*), we found that varying γ_{AR} leads to significant changes in zone brightness but no change in background intensity, which is inconsistent with Observations (O2)–(O3). Hence we explored the second possibility, that PKCη affects both inactivation rates $\bar{d}_R$ and $\bar{d}_C$ in equation (2.1*d*).

As before, we used the sharp switch model approximation (figure 4*a*) and numerical confirmation (figure 4*b*) to assess the influence of inactivation rates on Rho steady states. The model predicts that as inactivation strength decreases (e.g. from the hypothesized effect of PKCη DN), both zone intensity and background intensity increase. Increased background intensity is consistent with observation (O2). While zone intensity appears to be highly sensitive to the inactivation rate near $\bar{d}_R = 0$, in practice, we expect that basal components of the inactivation rate in equation (2.1*d*) bound the relevant parameter range away from zero. It is reasonable to assume that the relevant range of net inactivation rate resides beyond the grey band in figure 4*a*. Thus while our analysis points to an increase in zone intensity for PKCη DN, the change would be fairly small and would be similar in magnitude to the increase in background. Hence our model predictions are consistent with the hypothesis that PKCη negatively regulates GTPases by promoting their inactivation. (Similar conclusions would be found in a model where PKCη suppresses basal activation levels, omitted here.)

Up to this point, we have considered PKCη to be spatially homogeneous. Observations (O3)–(O4) however require us to revise this and take a more sophisticated view of how its spatial distribution influences zone formation. Imaging indicates that PKCη is spatially graded with the highest concentration near the wound edge [24]. To determine how this spatial distribution might influence zone formation, we analysed the joint dependence of steady states for Rho (green) and Cdc42 (red) on the parameter η (figure 4*c*). Here η represents the level of PKCη and $d_{\eta,i}$ its proportional contribution to inactivation of the two GTPases as per equation (2.1*d*). We set $G = 0$, which is equivalent to folding the GDI-mediated inactivation terms into the basal terms (d_R and d_C, respectively).

With η as the bifurcation parameter (figure 4*c*), we found three regimes (right to left): (1) at high η, the Rho/Abr and Cdc42 subsystems have a single, low, background steady-state level and neither Rho nor Cdc42 zone forms, (2) at intermediate η only the Cdc42 zone can form (only Cdc42 is bistable) and (3) at lower η, both Cdc42 and Rho zones are possible. In such a case, we would speculate that the control wound pattern is entirely contained within regime (3), permitting the formation of both zones. While a graded distribution is not required to account for zone formation in control cells, it is needed to explain why in PKCη OE, the remaining Cdc42 zone is no closer to the wound than in control cells (O3). If PKCη were homogeneous, and the OE manipulation effectively pushed the region near the wound into regime (2), the Cdc42 zone would be expected to form at the wound edge, inconsistent with observations. We thus hypothesize that the graded distribution stratifies the spatial domain so that near the wound edge, the system is in regime (1) and at intermediate distances it is in regime (2) (Grey bar under figure 4*c*.) In this scenario, no zone could form adjacent to the wound, but rather, a Cdc42 zone could form at intermediate distances (as it does in control cells), consistent with (O3).

While a graded PKCη distribution can account for Cdc42 zone localization in PKCη OE cells, its effect on inactivation rates alone does not explain zone inversion. In particular, it does not explain why the Rho zone is significantly further from the wound edge. The formation of this zone does imply that such distant regions of the wound repair field are in the Rho-permissive regime (3). What though drives the formation of this distant Rho zone in PKCη OE cells, why does it only occur in 20% of cases, and why does it not appear in control cells?

The answer emerges from closer inspection of fluorescence images. In PKCη OE, we find a broad halo of elevated Rho activity outside the Cdc42 zone, even in the 80% of cells with no inversion [9]. This observation supports the idea that PKCη OE not only affects GTPase inactivation rates, but also broadens the 'initial conditions' that set up Rho activity further from the wound. It then also follows that whether the zones invert (20% of cases) or not (remaining 80% of cells) simply depends on whether elevated Rho activity breaches thresholds required to initiate a Rho activity zone. In other words, while all PKCη OE cells have broad Rho-permissive regions, some cells stochastically form this distant Rho zone, while others do not.

To test the hypothesis that the spatially graded distribution of PKCη along with this broader halo of initial Rho activity is responsible for Observations (O3) and (O4), we numerically simulated the spatial PDEs with a graded PKCη distribution (grey curve, figure 4*d*) that stratifies the spatial domain across regions (1)–(3). If the initial Rho distribution is broader than in controls, a zone inversion occurs, consistent with (O4). When the initial Rho distribution is narrower (as in control simulations, e.g. figure 3*e*), only the Cdc42 zone forms (results not shown) consistent with (O3). Combined, these results point to a scenario where PKCη sculpts the spatial profile of the Rho and Cdc42 zones, and these distant Rho zones result from both PKCη elevation and the secondary effects on initial Rho localization that coincide with OE.

3.5. Creating a 'playing field': possible role of guanosine nucleotide dissociation inhibitors

It is natural to ask what prevents the activity zones of GTPases from spreading laterally outwards, away from the wound, along the surface of the cell. Restated, we ask what defines the playing field within which the pattern formation takes place. As previously noted, reserves of inactive Rho and Cdc42 are not globally depleted when the wound-induced zones form. Indeed, multiple wounds made within just a few micrometres from each other elicit the same rapid formation of concentric Rho and Cdc42 zones [23]. Thus, depletion cannot be responsible for spatially limiting the extent of these zones as proposed in cell polarization involving the same GTPases [26–29]. What then is responsible for spatially limiting these zones of activity?

The idea we explore is that local conditions affect the availability of inactive GTPase in the periphery, for example, by rapid sequestration. GDIs are proteins that sequester GTPases and limit their activation by GEFs. The activity of GDIs is, in turn, modulated by at least two types of mechanisms: phosphorylation by various kinases including protein kinases C, and by the so-called GDI displacement factors (GDFs). Phosphorylation can reduce the affinity of GDIs for Rho, Rac and Cdc42, depending on the kinase in question and the site(s) of

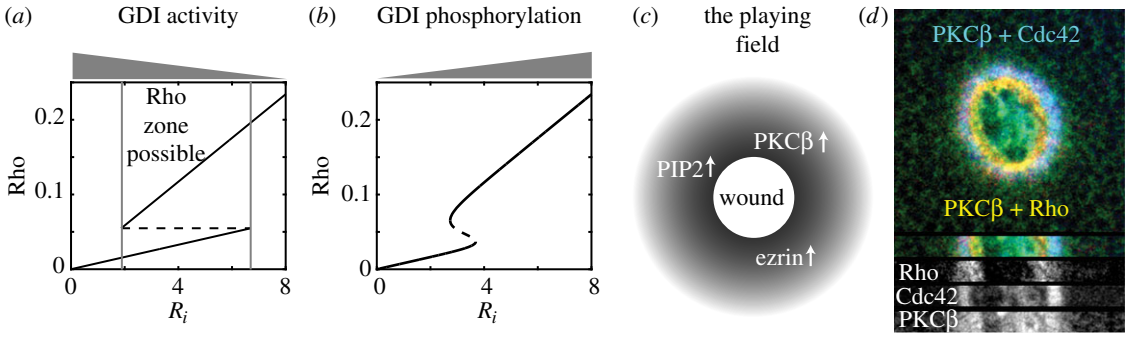

Figure 5. Modulating GDI creates the playing field. Modulating the level of locally activatable GTPase can abrogate or permit zone formation. (*a*,*b*) Bifurcation analysis of the sharp switch (*a*) and continuous (*b*) system with respect to R_i (level of activatable Rho), showing GDI and GDF activities (graded schematics) that could set up such variation of R_i towards the wound. The regime of bistability is consistent with zone formation, whereas levels of R_i outside that range are not. Increased GDI phosphorylation (which decreases its activity) or increased GDF concentration could both lead to an increase in R_i. Parameters are as in table 1 with $\bar{d}_R = 1.1$ and $\bar{d}_C = 0.4741$. (*c*) Schematic of the playing field hypothesis, indicating wound-associated factors that could influence GDI activity and hence affect R_i. If the strength of these factors decays away from the wound (e.g. on a diffusive length scale) it could create a locally permissive region (playing field) for Rho and Cdc42 zone formation. (*d*) Triple label showing the joint localization profiles of Rho (red), Cdc42 (blue) and PKCβ (green). The aqua colour indicates the overlap of Cdc42 and PKCβ flourescence channels (blue + green) while yellow indicates overlap of Rho and PKCβ fluorescence channels (red + green). Four slices through the wound diameter show the three signals overlapped, and then Rho, Cdc42 and PKCβ individually. The green stain in the middle of the wound is autofluorescence, which should be ignored. (Online version in colour.)

phosphorylation [30,31]. GDFs, which include PIP_2 and members of the ERM (ezrin, radixin and moesin) family, have been reported to promote the release of GTPases by GDI in the presence of GEFs (e.g. [32,33]). Given that both PKCs and PIP_2 concentrate around wounds, overlapping the regions occupied by the GTPase zones [24] (figure 5) it is reasonable to postulate that playing field establishment might reflect local antagonism of GDI. That is, the net effect of having relatively high local PKC activity and local accumulation of PIP_2 or other GDFs could locally depress sequestration of GTPases by GDI and thus increase levels of available inactive GTPases near the wound.

As an initial test of these ideas, we simply asked how the availability of inactive GTPases, represented by the parameters R_i, C_i in the model, influence zone formation. Restated, we asked over what range of values of these parameters is bistability (the hallmark of coexistence of zones and background levels) possible. In figure 5, we show model bifurcation plots with respect to R_i in both 'sharp switch' and continuous model variants (figure 5*a*,*b*, respectively). We find bistability only at intermediate values of R_i (and similarly for C_i, not shown).

We can interpret these results in terms of the GDI playing field hypothesis. For uninjured cells, the sequestering activity of GDI is spatially uniform and relatively strong, sequestering Cdc42 and Rho to such an extent that insufficient GTPase is available to initiate zone formation. Thus, while the GTPases are present in sufficient quantity throughout the cell, GDI sequestration reduces the available GTPase levels R_i, C_i (leftmost regime, figure 5*a*,*b*) and prevents zone formation. Upon wounding, the recruitment of PKCs and PIP_2 results in local suppression of GDI's sequestering activity and commensurate increases in R_i, C_i, making the wound region permissive to zone formation (middle regime, figure 5*a*,*b*). Since PKCs and GDFs are membrane-bound and concentrated near the wound, they do not alter the normal low levels of R_i and C_i in other regions of the cell, preventing the spread of the zones further afield. Hence, localized suppression of GDI activity in the model is consistent with higher levels of R_i, C_i near the wound, and with the idea that GDI helps to define a local playing field in which the patterns could form.

More detailed models and future experiments could be adapted to explore the link between GDI and the playing field hypothesis. Here we speculate that local recruitment of factors such as GDFs and PKCβ to the membrane near the wound (figure 5*c*), together with characteristic unbinding rates α, and diffusion rates D generate local gradient(s) of permissive factors that decay away from the wound edge with an effective length scale of $\sqrt{D/\alpha}$. This could define the spatial extent of the playing field. The 10 µm size of the region of zone formation is consistent with common diffusion length scales. Hence, it seems reasonable to suggest that wounding leads to the local release of sequestered GTPases that can then be activated and that participate in the healing process.

4. Discussion

In this review, we demonstrated how an interdisciplinary approach, using both biological experiments and mathematical modelling, improved our understanding of the mechanisms at play in single-cell wound patterning by Rho GTPases. Much like the canonical polarity response preceding chemotaxis [34,35], cell wound repair requires proper localization of small Rho GTPases (Cdc42 and Rho in this case) to direct cytoskeleton assembly and contraction. The approximate analytical and numerical methods described here, in combination with biological experiments [18,22,24,36] have been essential to understanding the molecular mechanisms regulating the repair response.

Based on results here and in previous investigations [9,23], we posit that wounding induces a multi-layered response where (1) local modulation of GDI activity generates a region near the wound (the so-called playing field) permissive to GTPase activation, (2) within that region, interactions between Rho, Cdc42 and Abr generate spatially patterned regions of activity and (3) PKCs modulate and fine-tune that activity. The first aspect of this hypothesis is based on the observations that (I) once initiated, GTPase zones do not spread away from the wound, (II) GDI modulation would provide a mechanism for controlling the system's capacity for bistability (and hence zone formation), and (III) multiple factors (PKCβ, ezrin, PIP_2)

which are known to weaken GDI's suppressive effects (at least in other systems) are recruited to the cell membrane near the wound.

The interactions between Rho, Cdc42 and Abr were fleshed out by comparing a collection of models, each encoding different hypothesized interactions, to observations from experiments manipulating Abr and Rho activities [23]. In particular, this modelling predicted that positive feedback of Cdc42 onto its own activation is essential to the process. Finally, our modelling [9] in combination with experimental manipulations [24] reveal specific roles of two GTPase effectors, PKCβ and PKCη. Based on semi-quantitative observations of how background and zone intensities change when these effectors are overexpressed (OE) or depressed (DN), we were able to rule out some plausible mechanisms. In the present case, we showed that PKCβ is unlikely to act on basal rates of activation, and more likely acts by enhancing both the positive feedback from Rho to itself via Abr and the auto-catalytic Cdc42 feedback. Furthermore, we were able to show that, as a result of being spatially graded, PKCη differentially affects Rho and Cdc42 at different distances from the wound, and that this is critical to account for the inversion of the Cdc42 and Rho zones obseved in some PKCη OE treatments.

The single-cell wound response is a dynamic process occurring over the course of minutes, with zones interacting and moving due to wound closure. Even so, the analysis of steady states herein provide insights into what drives the initial patterning. Using our one-dimensional spatial representation, we have demonstrated that it led us to reject some plausible hypotheses for the molecular mechanisms governing that patterning. From a mathematical perspective, the sharp switch approximation adopted here facilitated a more thorough exploration of parameter space, generating predictions that were confirmed with full numerical simulations. Future refinements of this modelling will be aimed at more fully understanding the role of GDIs and their phosphorylation, and identification of other GEFs and GAPs that modulate the GTPases during the repair process. At the same time, having mapped out regimes of behaviour, our model is ready for more sophisticated simulation methods in two and three dimensions that could describe the spherical cell geometry in a more accurate spatial representation.

Authors' contributions. W.R.H. and L.E.K. performed the modelling. A.E.G. and W.M.B. performed the experiments. W.R.H., L.E.K. and W.M.B. wrote the manuscript.

Competing interests. We declare we have no competing interests.

Funding. L.E.K. would like to thank the Isaac Newton Institute for Mathematical Sciences for its hospitality during the programme *Coupling Geometric PDEs and Physics for Processes on Biological Surfaces* supported by EPSRC grant no. EP/K032208/1. W.R.H. was supported by NSF grant nos. DMS1562078 and SES1556325. L.E.K. is supported by an NSERC Discovery Grant. W.M.B. is supported by National Institutes of Health grant no. GM52932.

References

1. Turing AM. 1952 The chemical basis of morphogenesis. *Phil. Trans. R. Soc. Lond. B* **237**, 37–72. (doi:10.1098/rstb.1952.0012)
2. Meinhardt H. 1982 *Models of biological pattern formation*, vol. 6. London, UK: Academic Press.
3. Gierer A, Meinhardt H. 1972 A theory of biological pattern formation. *Kybernetik* **12**, 30–39. (doi:10.1007/BF00289234)
4. Meinhardt H. 1999 Orientation of chemotactic cells and growth cones: models and mechanisms. *J. Cell Sci.* **112**, 2867–2874.
5. Levchenko A, Iglesias PA. 2002 Models of eukaryotic gradient sensing: application to chemotaxis of amoebae and neutrophils. *Biophys. J.* **82**, 50–63. (doi:10.1016/S0006-3495(02)75373-3)
6. Ma L, Janetopoulos C, Yang L, Devreotes PN, Iglesias PA. 2004 Two complementary, local excitation, global inhibition mechanisms acting in parallel can explain the chemoattractant-induced regulation of PI (3, 4, 5) P 3 response in *Dictyostelium* cells. *Biophys. J.* **87**, 3764–3774. (doi:10.1529/biophysj.104.045484)
7. Iglesias PA, Devreotes PN. 2008 Navigating through models of chemotaxis. *Curr. Opin. Cell Biol.* **20**, 35–40. (doi:10.1016/j.ceb.2007.11.011)
8. Otsuji M, Ishihara S, Kaibuchi K, Mochizuki A, Kuroda S. 2007 A mass conserved reaction–diffusion system captures properties of cell polarity. *PLoS Comput. Biol.* **3**, e108. (doi:10.1371/journal.pcbi.0030108)
9. Holmes WR, Liao L, Bement W, Edelstein-Keshet L. 2015 Modeling the roles of protein kinase Cβ and η in single-cell wound repair. *Mol. Biol. Cell* **26**, 4100–4108. (doi:10.1091/mbc.E15-06-0383)
10. Bishop AL, Alan H. 2000 Rho GTPases and their effector proteins. *Biochem. J.* **348**, 241–255. (doi:10.1042/bj3480241)
11. Bement WM, Miller AL, von Dassow G. 2006 Rho GTPase activity zones and transient contractile arrays. *Bioessays* **28**, 983–993. (doi:10.1002/bies.20477)
12. Rossman KL, Der CJ, Sondek J. 2005 GEF means go: turning on RHO GTPases with guanine nucleotide-exchange factors. *Nat. Rev. Mol. Cell Biol.* **6**, 167–180. (doi:10.1038/nrm1587)
13. Moon SY, Zheng Y. 2003 Rho GTPase-activating proteins in cell regulation. *Trends Cell Biol.* **13**, 13–22. (doi:10.1016/S0962-8924(02)00004-1)
14. DerMardirossian C, Bokoch GM. 2005 GDIs: central regulatory molecules in Rho GTPase activation. *Trends Cell Biol.* **15**, 356–363. (doi:10.1016/j.tcb.2005.05.001)
15. Guilluy C, Garcia-Mata R, Burridge K. 2011 Rho protein crosstalk: another social network? *Trends Cell Biol.* **21**, 718–726. (doi:10.1016/j.tcb.2011.08.002)
16. Bement WM, von Dassow G. 2014 Single cell pattern formation and transient cytoskeletal arrays. *Curr. Opin. Cell Biol.* **26**, 51–59. (doi:10.1016/j.ceb.2013.09.005)
17. Holmes WR, Edelstein-Keshet L. 2016 Analysis of a minimal Rho-GTPase circuit regulating cell shape. *Phys. Biol.* **13**, 046001. (doi:10.1088/1478-3975/13/4/046001)
18. Benink HA, Bement WM. 2005 Concentric zones of active RhoA and Cdc42 around single cell wounds. *J. Cell Biol.* **168**, 429–439. (doi:10.1083/jcb.200411109)
19. Abreu-Blanco MT, Verboon JM, Parkhurst SM. 2014 Coordination of Rho family GTPase activities to orchestrate cytoskeleton responses during cell wound repair. *Curr. Biol.* **24**, 144–155. (doi:10.1016/j.cub.2013.11.048)
20. Mandato CA, Bement WM. 2001 Contraction and polymerization cooperate to assemble and close actomyosin rings around Xenopus oocyte wounds. *J. Cell Biol.* **154**, 785–798. (doi:10.1083/jcb.200103105)
21. Chuang T, Xu X, Kaartinen V, Heisterkamp N, Groffen J, Bokoch G. 1995 Abr and Bcr are multifunctional regulators of the Rho GTP-binding protein family. *Proc. Natl Acad. Sci. USA* **92**, 10 282–10 286. (doi:10.1073/pnas.92.22.10282)
22. Vaughan EM, Miller AL, Hoi-Ying EY, Bement WM. 2011 Control of local Rho GTPase crosstalk by Abr. *Curr. Biol.* **21**, 270–277. (doi:10.1016/j.cub.2011.01.014)
23. Simon CM, Vaughan EM, Bement WM, Edelstein-Keshet L. 2013 Pattern formation of Rho GTPases in single cell wound healing. *Mol. Biol. Cell* **24**, 421–432. (doi:10.1091/mbc.E12-08-0634)

24. Vaughan EM, You JS, Yu HYE, Lasek A, Vitale N, Hornberger TA, Bement WM. 2014 Lipid domain-dependent regulation of single-cell wound repair. *Mol. Biol. Cell* **25**, 1867–1876. (doi:10.1091/mbc.E14-03-0839)
25. Liao L. 2013 Signalling in single cell wound healing. MSc thesis, University of British Columbia, Vancouver, Canada. See https://open.library.ubc.ca/clRcle/collections/ubctheses/24/items/1.0074055.
26. Mori Y, Jilkine A, Edelstein-Keshet L. 2008 Wave-pinning and cell polarity from a bistable reaction-diffusion system. *Biophys. J.* **94**, 3684–3697. (doi:10.1529/biophysj.107.120824)
27. Edelstein-Keshet L, Holmes WR, Zajac M, Dutot M. 2013 From simple to detailed models for cell polarization. *Phil. Trans. R. Soc. B* **368**, 20130003. (doi:10.1098/rstb.2013.0003)
28. Holmes WR, Lin B, Levchenko A, Edelstein-Keshet L. 2012 Modelling cell polarization driven by synthetic spatially graded Rac activation. *PLoS Comput. Biol.* **8**, e1002366. (doi:10.1371/journal.pcbi.1002366)
29. Lin B, Holmes WR, Wang J, Ueno T, Harwell A, Edelstein-Keshet L, Inoue T, Levchenko A. 2012 Synthetic spatially graded Rac activation drives directed cell polarization and locomotion. *Proc. Natl Acad. Sci. USA* **109**, E3668–E3677. (doi:10.1073/pnas.1210295109)
30. Dovas A, Choi Y, Yoneda A, Multhaupt HA, Kwon SH, Kang D, Oh E-S, Couchman JR. 2010 Serine 34 phosphorylation of rho guanine dissociation inhibitor (RhoGDIα) links signaling from conventional protein kinase C to RhoGTPase in cell adhesion. *J. Biol. Chem.* **285**, 23 296–23 308. (doi:10.1074/jbc.M109.098129)
31. Griner EM, Churchill ME, Brautigan DL, Theodorescu D. 2013 PKCα phosphorylation of RhoGDI2 at Ser31 disrupts interactions with Rac1 and decreases GDI activity. *Oncogene* **32**, 1010–1017. (doi:10.1038/onc.2012.124)
32. Takahashi K, Sasaki T, Mammoto A, Takaishi K, Kameyama T, Tsukita S, Takai Y. 1997 Direct interaction of the Rho GDP dissociation inhibitor with ezrin/radixin/moesin initiates the activation of the Rho small G protein. *J. Biol. Chem.* **272**, 23 371–23 375. (doi:10.1074/jbc.272.37.23371)
33. Fauré J, Vignais PV, Dagher MC. 1999 Phosphoinositide-dependent activation of Rho A involves partial opening of the RhoA/Rho-GDI complex. *Eur. J. Biochem.* **262**, 879–889. (doi:10.1046/j.1432-1327.1999.00458.x)
34. Jilkine A, Edelstein-Keshet L. 2011 A comparison of mathematical models for polarization of single eukaryotic cells in response to guided cues. *PLoS Comput. Biol.* **7**, e1001121. (doi:10.1371/journal.pcbi.1001121)
35. Holmes WR, Edelstein-Keshet L. 2012 A comparison of computational models for eukaryotic cell shape and motility. *PLoS Comput. Biol.* **8**, e1002793. (doi:10.1371/journal.pcbi.1002793)
36. Sonnemann KJ, Bement WM. 2011 Wound repair: toward understanding and integration of single-cell and multicellular wound responses. *Annu. Rev. Cell Dev. Biol.* **27**, 237–263. (doi:10.1146/annurev-cellbio-092910-154251)